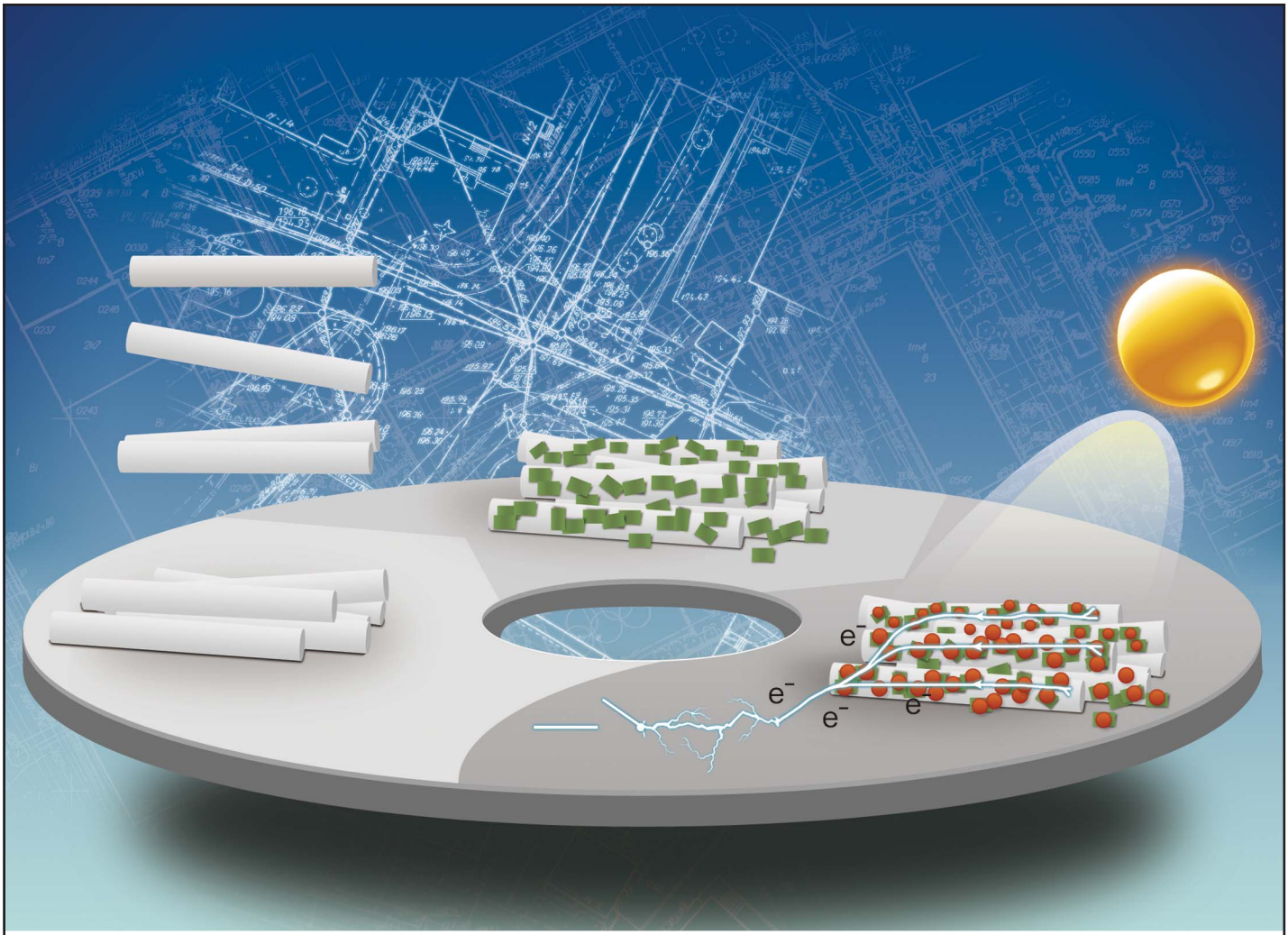

Showcasing the research of quantum dot sensitized solar cells from Prof. J.J.Tian's and Prof. G.Z.Cao's lab, University of Science and Technology Beijing, China, and University of Washington, the United States.

Title: ZnO/TiO_2 nanocable structured photoelectrodes for CdS/CdSe quantum dot co-sensitized solar cells

A hierarchical structure of ZnO/TiO_2 nanocable photoanode for quantum dot sensitized solar cells (QDSC) was prepared by chemical precipitation method, which can efficiently absorb more amounts of quantum dots and suppress the charge recombination. As a result, the power conversion efficiency of QDSC was increased by 125%.

As featured in:

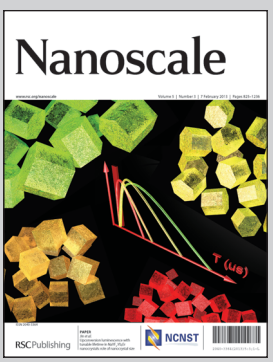

See Cao *et al.*, *Nanoscale*, 2013, **5**, 936.

RSC Publishing

www.rsc.org/nanoscale

Registered Charity Number 207890

Nanoscale

RSC Publishing

PAPER

ZnO/TiO_2 nanocable structured photoelectrodes for CdS/CdSe quantum dot co-sensitized solar cells

Cite this: *Nanoscale*, 2013, **5**, 936

Jianjun Tian,*[ab] Qifeng Zhang,[b] Lili Zhang,[b] Rui Gao,[b] Laifa Shen,[b] Shengen Zhang,[a] Xuanhui Qu[a] and Guozhong Cao*[b]

Photoelectrode made of nanocable structure of ZnO nanorods (NR) coated with TiO_2 nanosheets (NSs) was investigated for CdS/CdSe quantum dot co-sensitized solar cells. ZnO NRs prepared solution reaction at 60 °C served as the backbone for direct electron transport in view of the single crystallinity of the ZnO NRs and the high electron mobility of ZnO semiconductor. Anatase TiO_2 NSs with the thickness of ~10 nm and the length of ~100 nm were assembled onto the surface of ZnO NRs *via* a solvothermal method. It was found that the thin shell of TiO_2 might have remarkable influence on the quantum dot sensitized solar cells (QDSCs) through (a) increasing the surface area of ZnO NRs to allow for adsorbing more quantum dots (QDs), which led to high short current density, (b) forming an energy barrier that hindered the electrons in the ZnO from being back to the electrolyte and QDs, and thus, reduced the charge recombination rate, resulting in prolonged electron lifetime and enhanced open voltage. In comparison with the case of ZnO NRs, the short-circuit current density, open-circuit voltage, fill factor and charge recombination resistance of ZnO/TiO_2 nanocable photoelectrode increase by 3%, 44%, 48% and 220%, respectively. As a result, a power conversion efficiency of 2.7% of QDSCs with core–shell structural nanocable photoelectrode has been obtained, which is as much as 230% of that of 1.2% obtained for ZnO NR photoelectrode.

Received 7th September 2012
Accepted 31st October 2012

DOI: 10.1039/c2nr32663a

www.rsc.org/nanoscale

Introduction

Quantum dot sensitized solar cells (QDSCs) can be regarded as a derivative of dye-sensitized solar cells (DSCs); the latter has attracted world-wide scientific and technological interest since the breakthrough work done by O'Regan and Grätzel in 1991[1] for low cost solar cells compared to silicon-based solar cells.[2,3] To enhance light harvesting of DSCs in the visible region, many efforts have been made by focusing mainly on the development of high performance sensitizers.[4–7] Narrow-band-gap semiconductor quantum dots (QDs), such as CdS,[8,9] CdSe,[10,11] PbS[12] and InAs,[13] as next-generation sensitizers are considered more promising because of their extraordinary optical and electrical properties in terms of: (1) tunable band gap upon QD size, (2) high extinction coefficient, and (3) large intrinsic dipole moment which may facilitate charge separation in solar cells.[14–17] Moreover, theoretical photovoltaic conversion efficiency of QD-sensitized solar cells can reach up to 44% in view of multiple exciton generation (MEG) of QDs originating from quantum confinement effect.[18]

The porous nature of nanocrystalline TiO_2 films in combination with its electronic configuration drives their use in DSCs due to the large surface area available for dye-molecule adsorption, which is commonly used for the photoelectrode of QDSCs. ZnO is a good alternative of TiO_2 because it possesses an energy-band structure and physical properties similar to those of TiO_2, but has an electronic mobility ~4 times higher than that of TiO_2.[19–21] In addition, ZnO is easy to form anisotropic structure (such as nanowires, nanorods and nanotubes) presenting unique electronic and optical properties,[22,23] and furthermore, in view of much bigger size of QDs than that of dye molecules,[24] a photoelectrode film constructed with these nanostructures is helpful for the distribution of QDs. Recently, many studies have already been reported on a use of ZnO nanowire arrays for the application in QDSCs.[25–28] However, in literature,[26] the highest power conversion efficiency of the ZnO based QDSCs is ~3.6%, which is still lower than that of TiO_2-based one, being reflected by poor fill factor (FF) of the former. It has been recognized that the charge recombination is one of the main issues to deteriorate the FF of a solar cell, through a process known to occur by transferring the electrons in ZnO to the oxidized ions in the electrolyte. For the DSCs, many research results showed that the charge recombination could be reduced by applying a core–shell configuration.[29,30] Such a core–shell configuration is expected to suppress the charge recombination by forming an energy barrier to prevent the electrons in the

[a]*Advanced Material and Technology Institute, University of Science and Technology, Beijing, 100083, P.R. China. E-mail: jianjun2003@gmail.com; Fax: +86-10-62333375; Tel: +86-10-82376835*

[b]*Department of Materials and Engineering, University of Washington, Seattle, WA 98195-2120, USA. E-mail: gzcao@u.washington.edu; Fax: +1 206-543-3100; Tel: +1 206-616-9084*

conduction band of the semiconductor from transferring to the oxidized dyes and ions in the electrolyte, leading to increased open circuit voltage and short current density.[29–31] It was also reported[32] that the shell (TiO_2) has a more negative conduction band edge than that of the core oxide (ZnO) or it creates a dipole at the core–shell interface that shifts the band edge of the core upward in energy, which suppresses recombination and increases the open voltage and fill factor. Many novel core–shell structures, for example, ZnO/TiO_2, ZnO/Al_2O_3, ZnO/ZrO_2 and ZnO/MgO photoelectrodes, have been used in DSCs for this purpose.[29–33] Although the charge recombination of QDSCs was thought to be a little different from that of DSCs,[34] we believe that the introduction of a shell structure as energy barrier can also work for preventing the electrons from transferring to the electrolyte and therefore improve the performance of QDSCs.

In this work, we designed a core–shell structure consisting of ZnO nanorod (NR) coated with TiO_2 nanosheets (NSs). In addition to establishing an energy barrier, TiO_2 NSs might also enhance the surface area of the photoelectrode film for accommodating more QDs. Therefore, it is anticipated that such a core–shell configuration would enhance both the short-circuit current density (J_{sc}) and the open-circuit voltage (V_{oc}) as well as to increase FF of the solar cells. In view of high potential in the light harvest in a visible-light region[15] with high PCE reported,[35–38] CdS/CdSe QD is selected as co-sensitizer for QDSCs in this study. Fig. 1 is a schematic drawing showing the formation of quantum dot sensitized ZnO/TiO_2 nanocable photoelectrode film. In comparison with ZnO NR photoelectrode, the recombination resistance, V_{oc} and FF of core–shell structural QDSC increase by 220%, 44% and 48%, respectively. PCE of the QDSCs reaches to 2.7%, which is more than twice times that of 1.2% for ZnO NRs. Possible mechanisms for such enhancement in the power conversion efficiency have been discussed.

Experimental procedure

ZnO NR was prepared on a FTO glass substrate by solution reaction in 0.015 M zinc nitrate and hexamethylenetetramine (HMT) aqueous solution as reported previously.[39] The FTO glass cleaned was placed in the aqueous solution, and solution reaction was carried out at 60 °C for 12 h. Then the ZnO NR-coated substrate was taken out and dried at 70 °C. The as-received substrate underwent a sintering process in air at 350 °C for 30 min.

ZnO/TiO_2 core–shell nanocable was synthesized *via* solvothermal method using diethylenetriamine (DETA), isopropyl alcohol (IPA) and titanium isopropoxide (TIP) following a previously reported procedure.[40] Three solutions were prepared with different concentration: (I) 3.0 μM DETA and 0.05 mM TIP dissolved in 14 mL IPA; (II) 5.0 μM DETA and 0.09 mM TIP dissolved in 14 mL IPA; and (III) 7.0 μM DETA and 0.13 mM TIP dissolved in 14 mL IPA. The ZnO NR substrates and solutions were put in Teflon-lined stainless steel autoclaves and kept in an electric oven at 200 °C for 24 h. And then the autoclaves were taken out of oven and cooled to room temperature. The substrates were drained out of solution, washed carefully with ethanol, and calcined at 450 °C for 30 min. At last, the substrates with ZnO NR/TiO_2 NS core–shell structure were obtained.

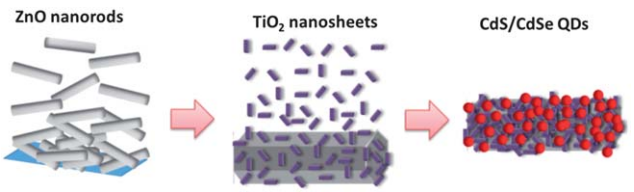

Fig. 1 Schematic of experimental process for ZnO/TiO_2 core–shell structure nanocable.

For the growth of CdS quantum dots, firstly, the substrates were immersed into a 0.1 M cadmium nitrate ($Cd(NO_3)_2$) methanol solution for 1 min. Successively, the substrates were dipped into a 0.1 M sodium sulfide (Na_2S) methanol solution for another 1 min to allow S^{2-} to react with the pre-adsorbed Cd^{2+}, leading to the formation of CdS. This procedure was called one SILAR cycle. In total six cycles were employed to obtain suitable amount of CdS on the TiO_2 film. In a sequent step, CdSe was deposited on the CdS coated substrates through a CBD method. Briefly, 0.1 M sodium selenosulphate (Na_2SeSO_3) aqueous, 0.1 M cadmium acetate $Cd(CH_2COO)_2$ aqueous solution and 0.2 M trisodium salt of nitrilotriacetic acid ($N(CH_2COONa)_3$) solution were mixed together with volume ratio 1 : 1 : 1. Then the CdS coated substrates were vertically immersed into the solution for the deposition of CdSe layer under dark condition at 24 °C for 4 h. After the deposition of CdSe, a ZnS passivation layer was deposited by two SILAR cycles while being soaking in an aqueous solution containing 0.1 M zinc nitrate and 0.1 M sodium sulfide, which act as Zn^{2+} and S^{2-} sources, respectively. Electrolyte employed in this study was composed of 1 M S and 1 M Na_2S in deionized water. Counter electrode is a Cu_2S film fabricated on brass foil. The preparation of Cu_2S electrode can be described as follows: brass foil was immersed into 37% HCl at 70 °C for 5 min, then rinsed with water and dried in air. After that, the etched brass foil was dipped into 1 M S and 1 M Na_2S aqueous solution, resulting in a black Cu_2S layer forming on the foil.

The morphology was characterized by Scan Electron Microscope (SEM, JSM-7000) and Transmission Electron Microscope (TEM, Tecnai G2 F20). Crystallographic information for the samples was collected using powder X-ray diffraction (XRD, Philips PW1830 Diffractometer). Nitrogen sorption isotherms were measured using a Quantach-rome NOVA 4200e. Samples are degassed at 250 °C under vacuum for at least 6 hours prior to measurement. The multi-point Brunauer–Emmett–Teller (BET) method was used to deter-mine the specific surface area. The photovoltaic properties were measured using an HP 4155A programmable semiconductor parameter analyzer under AM 1.5 simulated sunlight with the power density of 100 mW cm^{-2}. Optical absorption (Perkin Elmer Lambda 900 UV/VIS/IR Spectrometer) was used to study the samples' light absorption properties. The electrochemical impedance spectroscopy (EIS) was carried out through the Solartron 1287A coupling with the Solartron 1260 FRA/impedance analyzer to investigate electronic and ionic processes in the QDSCs.

Results and discussion

Fig. 2 shows the SEM images of the ZnO NRs, and ZnO/TiO_2 core–shell structured nanocables. Fig. 2a and b reveal that the average length and diameter of nanorods are ~5 μm and ~400 nm, respectively. The large gaps and pores among the NRs are helpful for a thorough penetration of CdS/CdSe QDs (3–10 nm)[24] into the ZnO NR photoelectrode film. At this step of ZnO NR synthesis, HMT acts as a pH buffer and provides a slow and controlled supply of OH^-. It has been proposed that HMT reacts with water to produce ammonia, which in turn reacts with water to generate OH^-.[39,41] Zn^{2+} reacted with the OH^- generated by HMT to form NRs. As shown in Fig. 2c, the smooth surfaces of NR gradually become "rough" and to be surrounded by NSs, forming a "shell". The constituent NSs are clearly visible and shown to adopt random orientations in the magnification micrographs (Fig. 2f and h). However, an over high concentration of the reaction solution can urge NSs to assemble and form nanospheres as shown in Fig. 2g and h. The thickness and length of the NS are ~10 nm and ~100 nm, respectively. It has been reported[40] that (001) surfaces of TiO_2 are most effectively stabilized by the tridentate DETA in the solvothermal system of TIP solution, which prohibits their growth along the [001] direction. After prolonged reaction, the two-dimensional lateral growth of such facets produces large ultrathin NSs. During the synthesis process, the ultrathin NSs are highly flexible and thus can readily deposit onto the surface of ZnO NRs, forming the hierarchical ZnO/TiO_2 nanocables As shown in the nitrogen sorption isotherms (Fig. 3), the hierarchical structure of ZnO/TiO_2 nanocables has much higher BET surface area (26.4 $m^2\ g^{-1}$) than that of ZnO nanorods (12.7 $m^2\ g^{-1}$). So the assembled TiO_2 NS on the surface of ZnO NR increases the surface area of the photoelectrode film, which is helpful for QD loading.

Shown in Fig. 4 are XRD patterns of ZnO NR, ZnO NR/TiO_2 NS core–shell structure. The diffraction peak of (101) of anatase TiO_2 can be found in Fig. 4c and d (JCPDS card no. 21-1272). The diffraction intensity of (101) increases with increasing of the solution concentration. The other diffraction peaks of anatase TiO_2 was not clearly observed because the content of TiO_2 is probably too small to detect in XRD patterns. However, the observation of (101) peak of anatase TiO_2 is already a good evidence for crystal structure of TiO_2 on the ZnO NRs. In other words, the core–shell structure of ZnO NRs covered with anatase TiO_2 NSs can be obtained *via* the solvothermal method at the appropriate reaction condition and solution concentration.

Fig. 5 is the TEM and HRTEM images of ZnO/TiO_2 core–shell structure adsorbed with CdS/CdSe QDs. Under the TEM with low magnification, only a "rough" edge has been observed as shown in Fig. 5a. Analysis with a high-resolution TEM (HRTEM) revealed that such a rough edge resulted from CdSe and CdS QDs with particle size of ~6 nm adsorbing on the TiO_2-coated ZnO nanorods.

Fig. 6a shows the optical absorbance of the CdS/CdSe co-sensitized photoelectrodes of ZnO NR and ZnO/TiO_2 core–shell structure. It can be seen that the absorbance of the core–shell structure photoelectrode absorbed QDs is higher than that of ZnO NR, indicating that more amount of QDs is achieved. As

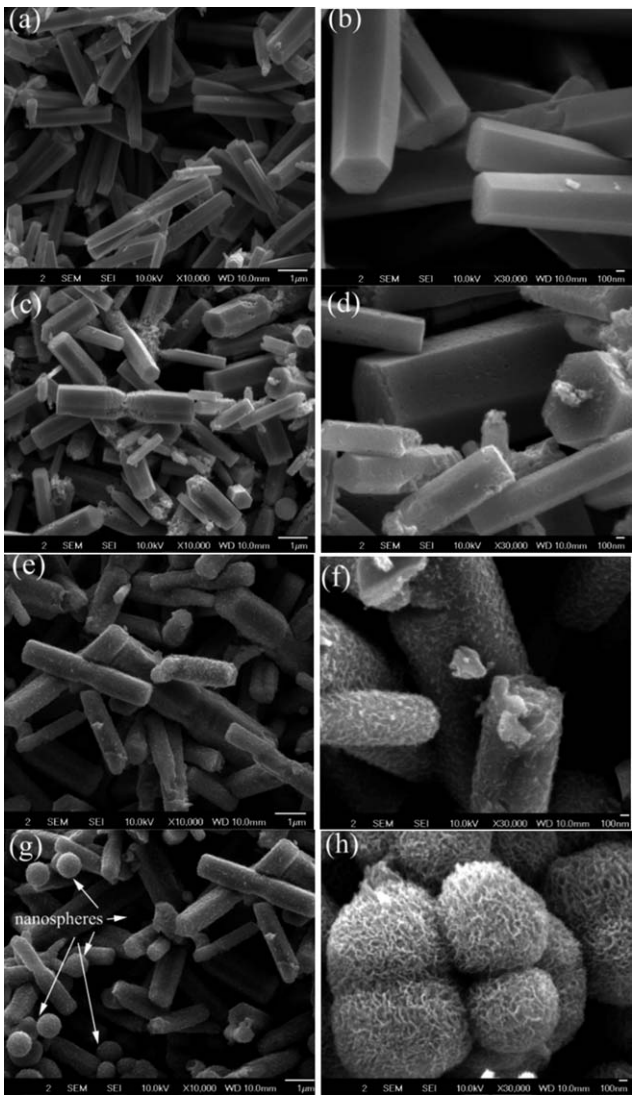

Fig. 2 SEM images of ZnO nanorods (a) and (b), ZnO/TiO_2 core–shell nanocables synthesized under different solution concentration: (c) and (d) of solution (I), (e) and (f) of solution (II), (g) and (h) of solution (III).

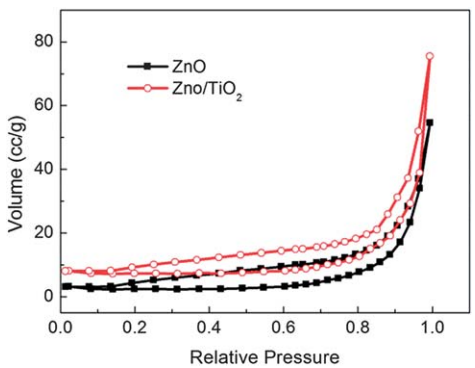

Fig. 3 Nitrogen sorption isotherms for the ZnO nanorods and ZnO/TiO_2 nanocables.

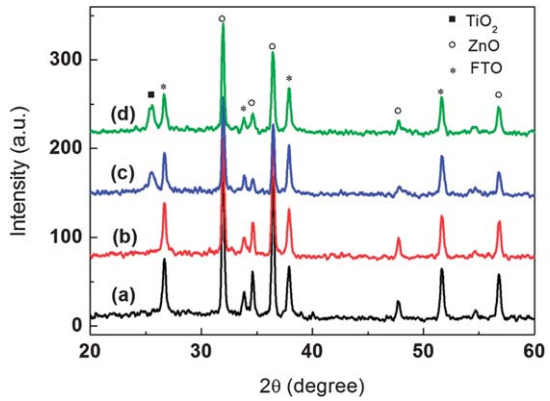

Fig. 4 XRD patterns of (a) ZnO NRs and ZnO/TiO_2 core–shell nanocables synthesized under different solution concentration (b) solution (I), (c) solution (II) and (d) solution (III).

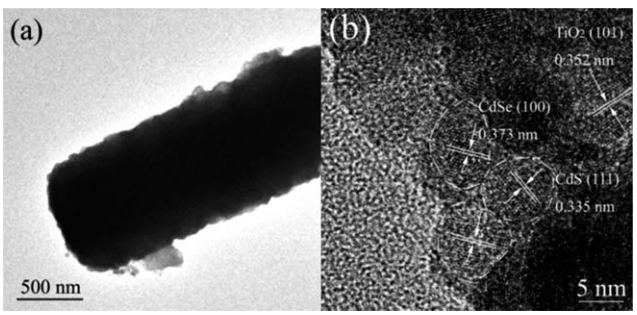

Fig. 5 TEM and HRTEM images of CdS/CdSe quantum dots on the ZnO/TiO_2 core–shell structured substrates.

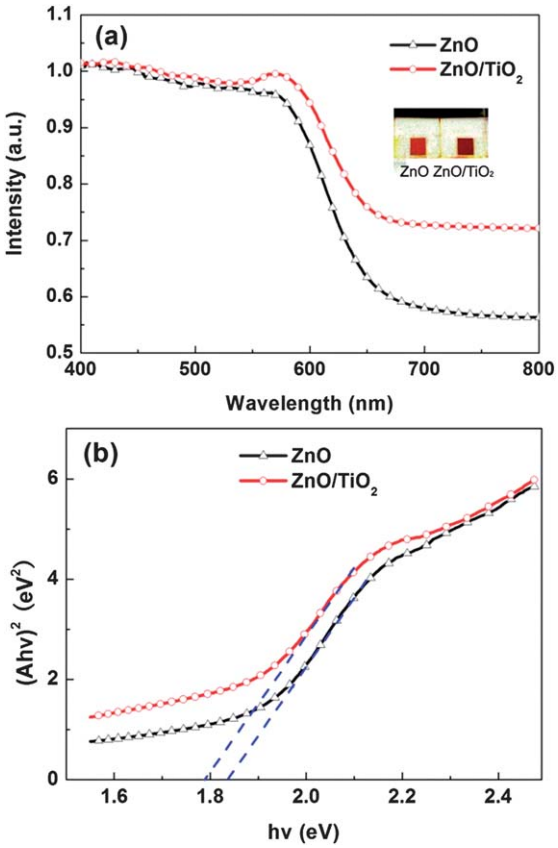

Fig. 6 (a) UV-Vis absorbance spectra and (b) $(Ahv)^2$ *vs. hv* curves of CdS/CdSe co-sensitized photoelectrodes of ZnO NR and ZnO/TiO_2 core–shell structure.

shown in the inset figure in Fig. 6a, much darker color of the ZnO/TiO_2 nanocable sample compared to that of ZnO nanorod sample implies the more amounts of QDs adsorbed onto the former than the latter. So TiO_2 NSs assembled on the surface of ZnO NRs, which increases the surface area and then enhances the harvesting amount of QDs. The shift of absorption edge of the ZnO/TiO_2 core–shell photoelectrode towards the long wavelength indicates that the QD particle size is bigger compared to the case of ZnO NRs. It is known that the optical band gap (E_g) for direct inter band transitions and the absorption coefficient (A) near the absorption edge has a relationship that complied with the following eqn (1):[42–44]

$$(Ahv)^2 = c\,(hv - E_g) \quad (1)$$

where the optical band gap for the absorption edge can be obtained by extrapolating the linear portion of the plot $(Ahv)^2$–hv to $A = 0$. E_g of CdSe can be obtained from Fig. 6b. The particle size of CdSe can be estimated using the eqn (2):[11,45]

$$\Delta E = E_1 - E_g = \frac{h^2}{8r^2}\left(\frac{1}{m_e} + \frac{1}{m_h}\right) \quad (2)$$

where ΔE is the band gap shift, r is the quantum dot radius, E_1 is the band gap of CdSe, E_g is the band gap of the bulk materials (1.7 eV for CdSe bulk material), m_e and m_h are the effective mass of electron and hole, respectively. For CdSe material, $m_e = 0.13m_0$ and $m_h = 0.44m_0$ ($m_0 = 9.11 \times 10^{-31}$ kg). The calculated particle sizes of CdSe on ZnO NR and ZnO/TiO_2 nanocable photoanodes are 5.4 nm and 6.8 nm, respectively. The result is in a good agreement with the HRTEM (Fig. 5b). The formation of CdSe QDs could be regarded through homogeneous nucleation during CBD process. So the size distribution of the nanoparticles is dependent on the subsequent growth process of the nuclei. The precursor solution concentration of core–shell is lower than that of ZnO NRs because ZnO NRs directly contact with the precursor solution. It was reported[46] that high concentration precursor solution has large number of initial nuclei formed in the nucleation stage, which results in smaller particle size. So CdSe QDs on the surface of ZnO NRs are smaller than that of ZnO/TiO_2 core–shell nanocables.

The photoelectrodes with different structures were employed to assemble solar cells. Fig. 7 shows the photocurrent–voltage (J–V) curves for the solar cells measured under the illumination of one sun (AM 1.5, 100 mW cm^{-2}). The performance parameters of the solar cells corresponding to Fig. 7, including open circuit voltage (V_{oc}), short circuit current density (J_{sc}), fill factor (FF) and power conversion efficiency (η), are listed in Table 1. Comparing with ZnO NR structure photoelectrode, the properties of ZnO/TiO_2 photoelectrode, including V_{oc}, J_{sc}, FF and η, increase evidently. The TiO_2 NSs assembled on the surface of ZnO NRs, which increases the surface area for *in situ* synthesis

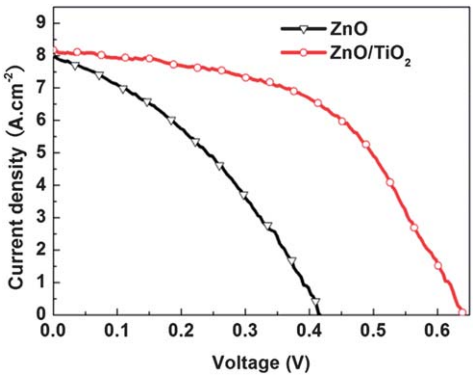

Fig. 7 *J–V* curves of ZnO NRs and ZnO/TiO_2 core–shell structural nanocables for QDSCs.

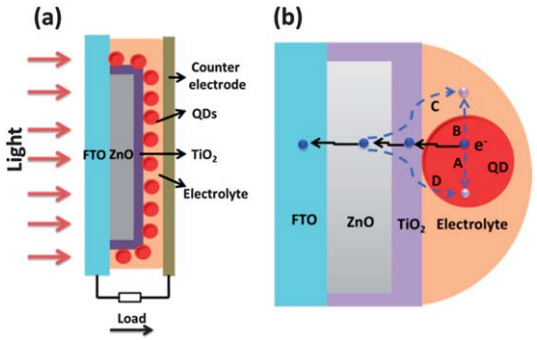

Fig. 8 Schemes of the structure of QDSC (a) and charge recombination pathways (b).

Table 1 Properties of ZnO NRs and ZnO/TiO_2 core–shell nanocables for QDSCs

Samples	V_{oc} (V)	J_{sc} (mA cm^{-2})	FF	η (%)
ZnO NRs	0.42	7.94	0.36	1.19
ZnO/TiO_2 nanocables	0.64	8.17	0.52	2.72

of QDs. So the increase of J_{sc} is mainly caused by the increase of QDs amount for more optical absorbance. The improvement of V_{oc} and FF mainly depended on the core–shell structure for high Fermi energy and low charge recombination. The Fermi energy of TiO_2 is higher than that of ZnO, resulting in larger V_{oc} of QDSCs. For the film constructed with ZnO nanorods, there is much large contact area between the ZnO surface and the electrolyte, which increases the recombination between the electron and the oxidized ions (Sn^{2-}) in electrolyte, leading to low open voltage of the solar cell can prevent electrons from entering the electrolyte and recombining with holes of electrolyte. As a result, the V_{oc}, FF and η increased by 44%, 48% and 130%, respectively.

Recently, a few studies focused on the charge recombination in QDSC due to its remarkable effect on the performance of the solar cells.[34,35,47–49] Fig. 8 shows the schemes of the structure of QDSC and charge recombination pathways in the solar cell. The cell structure of a CdS/CdSe co-sensitized quantum dot solar cell, which consists of an oxide nanocrystalline film, CdS/CdSe QD sensitizer, polysulfide electrolyte and counter electrode (as shown Fig. 8a). Under the operating conditions, photons are captured by QDs, yielding electron–hole pairs that are rapidly separated to electrons and holes at interface between the nanocrystalline oxide and QDs. The electrons inject into the oxide and holes are released by redox couples (S^{2-}/S_n^{2-}) in electrolyte. Compared to DSCs, the recombination in QDSCs is more complicated with several major pathways (as shown in Fig. 8b):[35,49] (A) recombination of electrons in the QD conduction band with holes in the QD valence band; (B) recombination with the electron acceptors in the electrolyte; (C) back electron injection from ZnO to electrolyte; (D) back electron injection from ZnO to QDs. Among these pathways, process (A) and (B) can be ignored in the QD due to the highly efficient charge separation. (C) and (D) recombination pathways can be considered the main factors that affect the performance of QDSC, depending on the interface resistance of oxide with electrolyte and QDs. In the case of ZnO/TiO_2 core–shell structure, TiO_2 shell could increase the interface resistance that leads to reducing the recombination through the mechanisms of (C) and (D). As shown in Fig. 9, the dark current of device based on ZnO/TiO_2 structure decreased compared to that of bare ZnO NRs, indicating a lower charge recombination from the conduction band of ZnO to the redox couple (S^{2-}/S_n^{2-}) in the electrolyte.

To evaluate the resistance distribution and charge recombination processes, the electrochemical impedance spectroscopy (EIS) measurements have been carried out. Fig. 10 shows the impedance spectra of the QDSCs measured under forward bias (−0.6 V) under dark condition. In Fig. 10a and b, the three semicircles correspond to the electron injection at the counter electrode (R1), the electron transfer at the photoelectrode–QDs–electrolyte interface and transport in the photoelectrode (R_2), and the transport of ions in the electrolyte, respectively.[50] A fitting result of the impedance spectra is listed in Table 2. The R_2 reflects electron recombination corresponding to the processes (C) and (D) in Fig. 8. Compare to ZnO NR, the R_2 of

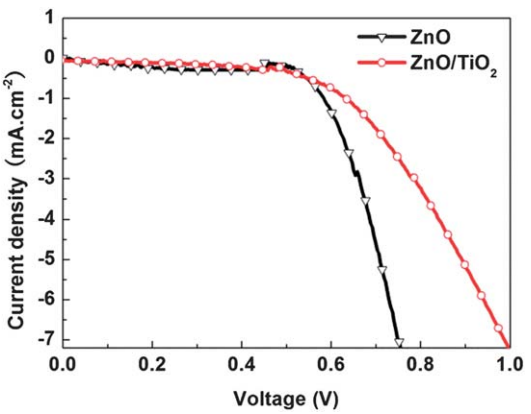

Fig. 9 *J–V* curves of ZnO NR and ZnO/TiO_2 core–shell structure for QDSCs under dark condition.

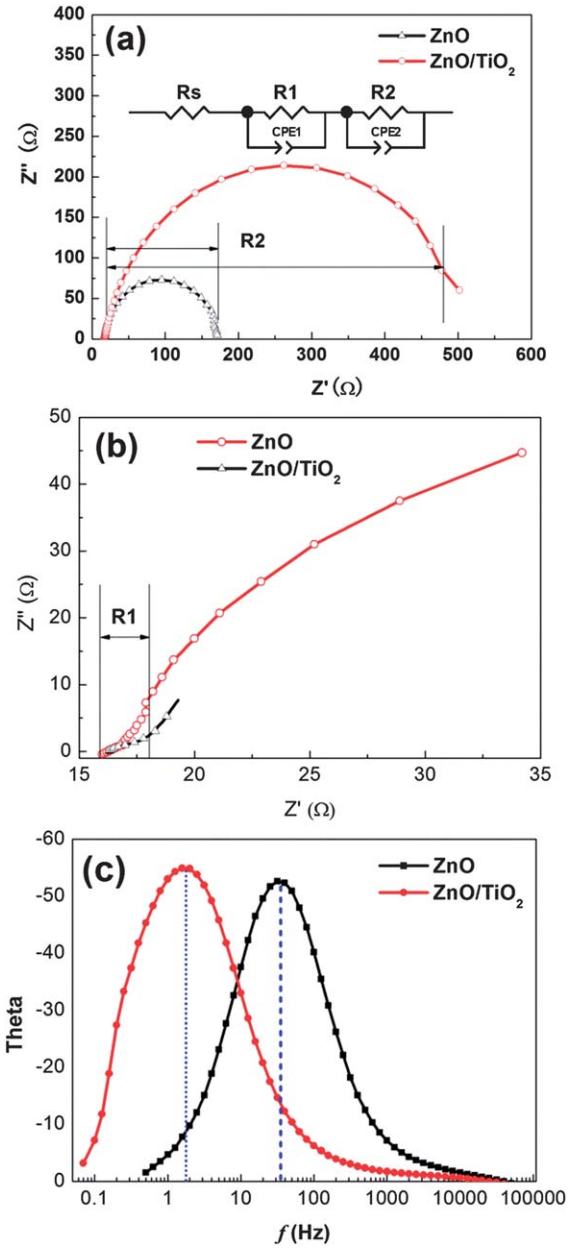

Fig. 10 EIS curves of QDSC with different structure: (a) and (b) Nyquist plots curves and (c) bode plots curves.

ZnO/TiO_2 core–shell structure increases from 153 Ω to 496 Ω, which increases by 220%. As the charge transfer resistance at the photoelectrode–electrolyte interface (R_2) includes the resistances of both the ZnO core and TiO_2 shell, the total charge transfer resistance for the core–shell structure can be written by eqn (3):[29]

Table 2 Electrochemical impedance results of QDSCs

Substrates	R_1 (Ω)	R_2 (Ω)	τ_n (ms)
ZnO NRs	15.9	153	5.1
ZnO/TiO_2 NRs	16.8	496	101

$$R_{total} = R_{core} + R_{shell} \quad (3)$$

where R_{core} and R_{shell} are the electron transfer resistances induced by the core and shell, respectively. So the result indicates that electrons in photoelectrode of ZnO/TiO_2 core–shell structure are more difficult to recombine in view of its high R_2. Fig. 10c shows the bode plots of QDSCs with different structure of photoelectrodes. The curve peak of the spectrum can be used to determine the electron lifetime in the ZnO according to the following eqn (4):[51]

$$\tau_n = \frac{1}{2\pi f_{min}} \quad (4)$$

The results are shown in Table 2, presenting that the electron lifetime of device of ZnO/TiO_2 core–shell photoelectrode is up to 101 ms, which is 20 times longer than that of ZnO NR (5.1 ms). In other words, the lifetime of electrons in the conduction band is prolonged due to the use of TiO_2 thin shell.

It is known that the charge recombination and electron lifetime have obvious impact on V_{oc}, FF and η for DSCs, and so do the QDSCs. The V_{oc} of a DSC can be expressed by eqn (5):[52,53]

$$V_{oc} = \frac{RT}{\beta F}\ln\left(\frac{AI}{n_0 k_b [I_3^-] + n_0 k_r [D^+]}\right) \quad (5)$$

where R is the molar gas constant, T is the temperature, F is the Faraday constant, β is the reaction order for I_3^- and electrons, A is the electrode area, I is the incident photon flux, n_0 is the concentration of accessible electronic states in the conduction band and k_b and k_r are the kinetic constant of the backreaction of the injected electrons with triiodide and the recombination of these electrons with oxidized dyes (D^+), respectively. For QDSCs, the redox couple is S^{2-}/S_n^{2-} instead of I^-/I_3^-. Considering that ω_{max} $(1/f_{min})$ is the same as the backreaction constant (k_b), and that the V_{oc} is dependent logarithmically on f_{min}. So the value of V_{oc} increases with the decrease of back reaction constant (as same as f_{min}). From Fig. 10c, the device of ZnO/TiO_2 core–shell photoelectrode has much lower f_{min} than that of ZnO NR photoelectrode. So, according to eqn (5), the device of core–shell photoelectrode should have higher V_{oc}, which is consistent with the measured results of J–V curves shown in Fig. 7 and Table 1.

The charge transfer resistance at the photoelectrode–electrolyte interface denoted as R_2 in Fig. 10a can be considered as part of a shunt resistance (R_{sh}) because it behaves like a diode on the applied bias voltage.[29] The R_{sh} relates to FF as the following eqn (6):[29]

$$FF = FF_0(1 - 1/R_{sh}) \quad (6)$$

where FF_0 is the theoretical maximum FF. From the EIS results, it can be inferred that the increase of FF of QDSC with ZnO/TiO_2 structural photoelectrode as shown in Fig. 7 is a result of increase in R_{sh}, by 220%. According to the discussions above, the employment of TiO_2 shell can not only increase the harvesting amount of QDs, but may also enhance the charge recombination resistance and prolong the electron lifetime, both of which contribute to improving the J_{sc}, FF and V_{oc} of

QDSCs. Compared to the QDSC constructed with ZnO NRs, the η of QDSC with ZnO/TiO_2 core–shell photoelectrode increases by 130%, and reaches the maximum value of 2.7%.

Conclusions

Photoelectrode with core–shell structure of ZnO/TiO_2 nanocable for CdS/CdSe quantum dot co-sensitized solar cells has demonstrated much enhancement in power conversion efficiency.

The use of TiO_2 NS shell offered several advantages for quantum dot sensitized solar cells (QDSCs) as follows: (a) increases surface area of ZnO NRs to help for harvesting more quantum dots (QDs), which leads to high short current density J_{sc}; (b) forms a layer of energy barrier blocking the electrons from transporting back to electrolyte and QDs, which reduces the charger recombination and increases fill factor (FF) of the QDSCs; (c) prolongs electron lifetime so as to enhance the open-circuit voltage V_{oc}. In comparison with ZnO NRs, the J_{sc}, V_{oc}, FF and charge recombination resistance R_2 of core–shell structured photoelectrode increase by 3%, 44%, 48% and 220%, respectively. As a result, a power conversion efficiency η of 2.7% of QDSCs with core–shell structural photoelectrode has been obtained, which is as much as 230% of that for ZnO NR photoelectrode (1.2%).

Acknowledgements

This work was supported by National Science Foundation of China (51004011 and 51174247), the Fundamental Research Funds for the Central Universities (FRF-TP-12-153A) and the U.S. Department of Energy, Office of Basic Energy Sciences, Division of Materials Sciences, under Award no. DE-FG02-07ER46467 (Q.F.Z.). This work is also supported in part by the National Science Foundation (DMR 1035196), the University of Washington TGIF grant, and the Royalty Research Fund (RRF) from the Office of Research at University of Washington.

Notes and references

1 B. O'Regan and M. Gratzel, *Nature*, 1991, **353**, 737–740.
2 C. J. Barbe, F. Arendse, P. Comte, M. Jirousek, F. Lenzmann, V. Shklover and M. Gratzel, *J. Am. Ceram. Soc.*, 1997, **80**, 3157–3171.
3 A. Yella, H. W. Lee, H. N. Tsao, C. Y. Yi, A. K. Chandiran, M. K. Nazeeruddin, E. W. G. Diau, C. Y. Yeh, S. M. Zakeeruddin and M. Gratzel, *Science*, 2011, **334**, 629–634.
4 T. Bessho, E. Yoneda, J. H. Yum, M. Guglielmi, I. Tavernelli, H. Imai, U. Rothlisberger, M. K. Nazeeruddin and M. Gratzel, *J. Am. Chem. Soc.*, 2009, **131**, 5930–5934.
5 P. G. Bomben, K. C. D. Robson, P. A. Sedach and C. P. Berlinguette, *Inorg. Chem.*, 2009, **48**, 9631–9643.
6 P. G. Johansson, J. G. Rowley, A. Taheri and G. J. Meyer, *Langmuir*, 2011, **27**, 14522–14531.
7 H. C. Zhao, J. P. Harney, Y. T. Huang, J. H. Yum, M. K. Nazeeruddin, M. Gratzel, M. K. Tsai and J. Rochford, *Inorg. Chem.*, 2012, **51**, 1–3.
8 J. Kim, H. Choi, C. Nahm, J. Moon, C. Kim, S. Nam, D.-R. Jung and B. Park, *J. Power Sources*, 2011, **196**, 10526–10531.
9 S. Panigrahi and D. Basak, *J. Colloid Interface Sci.*, 2011, **364**, 10–17.
10 I. Robel, V. Subramanian, M. Kuno and P. V. Kamat, *J. Am. Chem. Soc.*, 2006, **128**, 2385–2393.
11 Q. Shen, J. Kobayashi, L. J. Diguna and T. Toyoda, *J. Appl. Phys.*, 2008, **103**, 084304.
12 R. Plass, S. Pelet, J. Krueger, M. Gratzel and U. Bach, *J. Phys. Chem. B*, 2002, **106**, 7578–7580.
13 P. Yu, K. Zhu, A. G. Norman, S. Ferrere, A. J. Frank and A. J. Nozik, *J. Phys. Chem. B*, 2006, **110**, 25451–25454.
14 V. Gonzalez-Pedro, X. Xu, I. Mora-Sero and J. Bisquert, *ACS Nano*, 2010, **4**, 5783–5790.
15 G. Zhu, L. Pan, T. Xu and Z. Sun, *ACS Appl. Mater. Interfaces*, 2011, **3**, 3146–3151.
16 M. A. Hossain, J. R. Jennings, Z. Y. Koh and Q. Wang, *ACS Nano*, 2011, **5**, 3172–3181.
17 Z. X. Pan, H. Zhang, K. Cheng, Y. M. Hou, J. L. Hua and X. H. Zhong, *ACS Nano*, 2012, **6**, 3982–3991.
18 M. C. Hanna and A. J. Nozik, *J. Appl. Phys.*, 2006, **100**, 074510.
19 T. P. Chou, Q. F. Zhang, G. E. Fryxell and G. Z. Cao, *Adv. Mater.*, 2007, **19**, 2588–2592.
20 Q. F. Zhang and G. Z. Cao, *J. Mater. Chem.*, 2011, **21**, 6769–6774.
21 Q. F. Zhang, T. R. Chou, B. Russo, S. A. Jenekhe and G. Z. Cao, *Angew. Chem., Int. Ed.*, 2008, **47**, 2402–2406.
22 Q. F. Zhang, C. S. Dandeneau, X. Y. Zhou and G. Z. Cao, *Adv. Mater.*, 2009, **21**, 4087–4108.
23 Q. F. Zhang, S. Yodyingyong, J. T. Xi, D. Myers and G. Z. Cao, *Nanoscale*, 2012, **4**, 1436–1445.
24 J. J. Tian, R. Gao, Q. F. Zhang, S. G. Zhang, Y. W. Li, J. L. Lan, X. H. Qu and G. Z. Cao, *J. Phys. Chem. C*, 2012, **116**, 18655–18662.
25 M. Seol, H. Kim, Y. Tak and K. Yong, *Chem. Commun.*, 2010, **46**, 5521–5523.
26 M. Seol, E. Ramasamy, J. Lee and K. Yong, *J. Phys. Chem. C*, 2011, **115**, 22018–22024.
27 C.-Z. Yao, B.-H. Wei, L.-X. Meng, H. Li, Q.-J. Gong, H. Sun, H.-X. Ma and X.-H. Hu, *J. Power Sources*, 2012, **207**, 222–228.
28 T. Bora, H. H. Kyaw and J. Dutta, *Electrochim. Acta*, 2012, **68**, 141–145.
29 K. Park, Q. F. Zhang, B. B. Garcia and G. Z. Cao, *J. Phys. Chem. C*, 2011, **115**, 4927–4934.
30 K. Park, Q. F. Zhang, B. B. Garcia, X. Y. Zhou, Y. H. Jeong and G. Z. Cao, *Adv. Mater.*, 2010, **22**, 2329–2332.
31 M. L. Wang, C. G. Huang, Y. G. Cao, Q. J. Yu, Z. H. Deng, Y. Liu, Z. Huang, J. Q. Huang, Q. F. Huang, W. Guo and J. K. Liang, *J. Phys. D: Appl. Phys.*, 2009, **42**, 155104.
32 M. Law, L. E. Greene, A. Radenovic, T. Kuykendall, J. Liphardt and P. D. Yang, *J. Phys. Chem. B*, 2006, **110**, 22652–22663.

33 N. O. V. Plank, I. Howard, A. Rao, M. W. B. Wilson, C. Ducati, R. S. Mane, J. S. Bendall, R. R. M. Louca, N. C. Greenham, H. Miura, R. H. Friend, H. J. Snaith and M. E. Welland, *J. Phys. Chem. C*, 2009, **113**, 18515–18522.

34 I. Mora-Sero, S. Gimenez, F. Fabregat-Santiago, R. Gomez, Q. Shen, T. Toyoda and J. Bisquert, *Acc. Chem. Res.*, 2009, **42**, 1848–1857.

35 X.-Y. Yu, J.-Y. Liao, K.-Q. Qiu, D.-B. Kuang and C.-Y. Su, *ACS Nano*, 2011, **5**, 9494–9500.

36 Q. Zhang, X. Guo, X. Huang, S. Huang, D. Li, Y. Luo, Q. Shen, T. Toyoda and Q. Meng, *Phys. Chem. Chem. Phys.*, 2011, **13**, 4659–4667.

37 P. K. Santra and P. V. Kamat, *J. Am. Chem. Soc.*, 2012, **134**, 2508–2511.

38 T. Shu, Z. M. Zhou, H. Wang, G. H. Liu, P. Xiang, Y. G. Rong, H. W. Han and Y. D. Zhao, *J. Mater. Chem.*, 2012, **22**, 10525–10529.

39 H. P. Dong, L. D. Wang, R. Gao, B. B. Ma and Y. Qiu, *J. Mater. Chem.*, 2011, **21**, 19389–19394.

40 J. S. Chen, Y. L. Tan, C. M. Li, Y. L. Cheah, D. Y. Luan, S. Madhavi, F. Y. C. Boey, L. A. Archer and X. W. Lou, *J. Am. Chem. Soc.*, 2010, **132**, 6124–6130.

41 C. T. Wu, W. P. Liao and J. J. Wu, *J. Mater. Chem.*, 2011, **21**, 2871–2876.

42 R. Gao, L. Wang, Y. Geng, B. Ma, Y. Zhu, H. Dong and Y. Qiu, *Phys. Chem. Chem. Phys.*, 2011, **13**, 10635–10640.

43 R. Gao, L. Wang, Y. Geng, B. Ma, Y. Zhu, H. Dong and Y. Qiu, *J. Phys. Chem. C*, 2011, **115**, 17986–17992.

44 R. Gao, L. Wang, B. Ma, C. Zhan and Y. Qiu, *Langmuir*, 2010, **26**, 2460–2465.

45 Q. Shen and T. Toyoda, *Jpn. J. Appl. Phys.*, 2004, **43**, 2946–2951.

46 G. Cao and Y. Wang, *Nanostructures and Nanomaterials*, World Scientifics Publishing Co. Pte. Ltd., Singapore, 2011.

47 E. M. Barea, M. Shalom, S. Gimenez, I. Hod, I. Mora-Sero, A. Zaban and J. Bisquert, *J. Am. Chem. Soc.*, 2010, **132**, 6834–6839.

48 S. Emin, M. Yanagida, W. Q. Peng and L. Y. Han, *Sol. Energy Mater. Sol. Cells*, 2012, **101**, 5–10.

49 I. Hod, V. Gonzalez-Pedro, Z. Tachan, F. Fabregat-Santiago, I. Mora-Sero, J. Bisquert and A. Zaban, *J. Phys. Chem. Lett.*, 2011, **2**, 3032–3035.

50 N. Koide, A. Islam, Y. Chiba and L. Y. Han, *J. Photochem. Photobiol., A*, 2006, **182**, 296–305.

51 R. Kern, R. Sastrawan, J. Ferber, R. Stangl and J. Luther, *Electrochim. Acta*, 2002, **47**, 4213–4225.

52 Q. Wang, S. Ito, M. Gratzel, F. Fabregat-Santiago, I. Mora-Sero, J. Bisquert, T. Bessho and H. Imai, *J. Phys. Chem. B*, 2006, **110**, 25210–25221.

53 K. Lee, S. W. Park, M. J. Ko, K. Kim and N. G. Park, *Nat. Mater.*, 2009, **8**, 665–671.